

SESSIONE D MECCANICA DEI MATERIALI

RESISTANCE TO FATIGUE CRACK GROWTH AND CORROSION OF MAGNESIUM ALLOYS

G. Nicoletto^a, P. Lanfredi Sofia^a, B. Hadzimova^b, P. Palcek^b

^a *Dipartimento di Ingegneria Industriale, Università di Parma, Italy*
e-mail: nick@me.unipr.it

^b *Department of Materials Engineering, University of Žilina, Slovakia*

Abstract

Magnesium alloys have a great potential as construction materials for their many favourable technical and economical characteristics and many industrial sectors have shown an increased use in the recent years. In this paper fatigue crack growth tests and corrosion tests in four different environments on two Mg-alloys, namely AZ91 and AZ63HP, are reported.

The main conclusions of the fatigue crack growth tests are that both Mg-alloys show a limited influence of the R-ratio on the fatigue crack growth response in the Paris's law regime, although the AZ63HP reveals a larger scatter in the data. Threshold values of the ΔK are also similar for the two Mg-alloys.

As far as the corrosion tests it was found that corrosion rates of AZ63HP alloy are markedly higher than corrosion rates of AZ91 alloy. Furthermore corrosion rates in AZ91 alloy and in AZ63HP alloy increase going from the distilled water, to the normal water and to the river water. Finally, corrosion potentials and corrosion currents obtained in potentiodynamic tests coherently showed opposite trends in the four environments.

1. INTRODUCTION

Pure magnesium (Mg) has important characteristics such as very low density, corrosion resistance and vibration damping, but it is rarely used in practice because of its poor mechanical properties. Magnesium alloys, on the other hand, have a great potential as construction materials for their energy-efficient utilization, excellent specific strength, good casting properties, good machinability and weldability and low costs. Fig. 1 shows the Mg-based, Al-based materials and plastics production in the last century. Production of Mg-based materials is characterized by a sharp downturn in the fifties but presently it shows a steadily increasing trend, [1].

In addition to good relative mechanical properties, Mg-alloys have an excellent corrosion resistance when compared with other materials, [2]. In Fig. 2 corrosion tests in salt spray in different material are compared with the Mg-alloy showing the best performance. Sectors in which Mg-alloys are increasingly used are the automotive, aerospace, general mechanical, consumer products, consumer electronics.

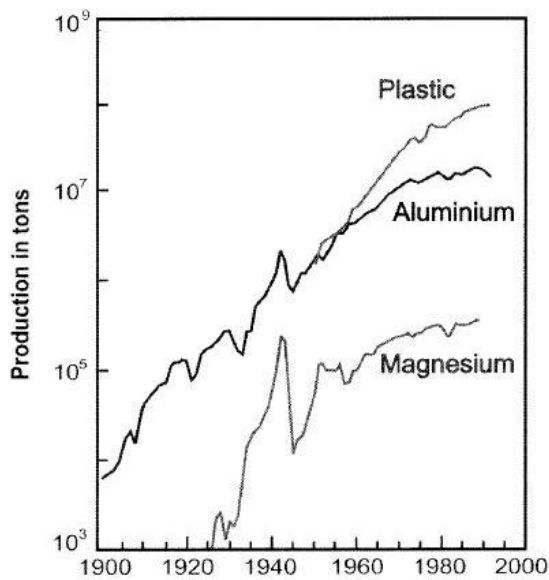


Fig. 1 - Trend in material production

Due to the practical interest in this class of materials, two Mg-alloys were characterized in terms of fatigue crack growth resistance and corrosion resistance in different environments. The main results are reported in this paper.

2. MATERIALS

The Mg-alloys under study have the following denomination: AZ91 and AZ63HP. Their chemical compositions are given in Tab.1. The materials tested in the as-cast conditions, [3].

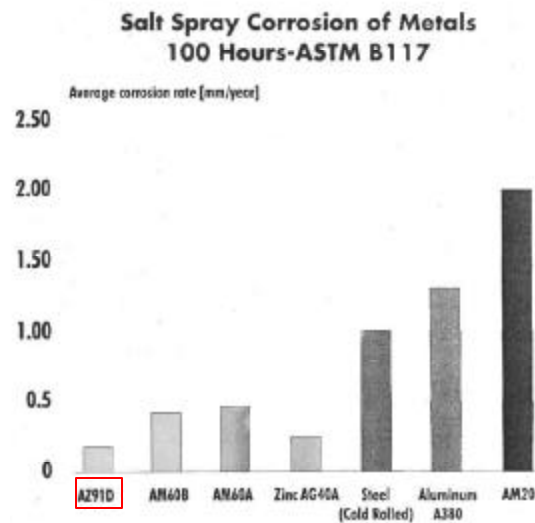


Fig. 2 – Comparison of the corrosion resistance of several materials

Tab.1- Chemical composition of the Mg Alloys tested

Mg- Alloy	Content of elements[wt.%]						
	Al	Zn	Mn	Si	Cu	Fe	Be
AZ91	8,03	0,53	0,18	0,064	0,035	0,012	0,0004
AZ63HP	6,14	2,54	0,22	0,005	0,006	0,005	0,0004

The binary diagram of the Al-Mg system is shown in Fig.1. The δ phase is the basic solid solution of aluminium in magnesium and it has a hexagonal lattice. The γ phase is the $Al_{12}Mg_{17}$ electronic compound, the R phase is the $Al_{30}Mg_{23}$ electronic compound and β phase is the Al_3Mg_2 electronic compound. The α phase is the basic solid solution of magnesium in aluminium [4,5].

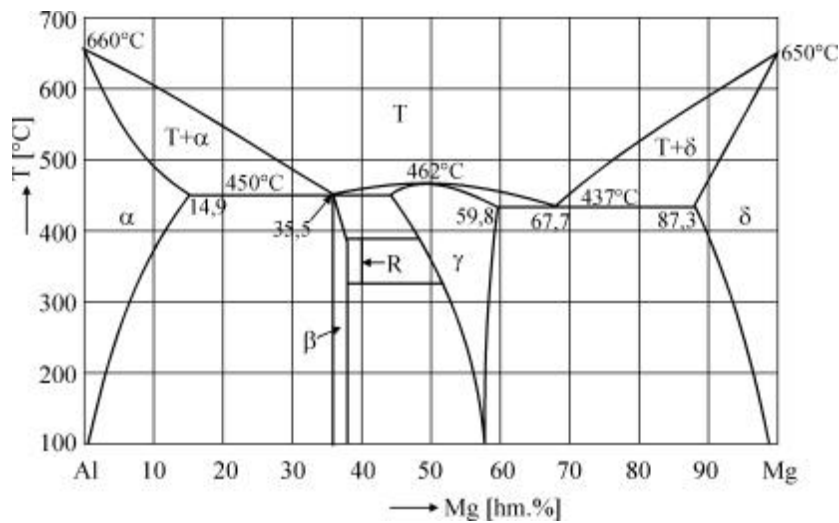
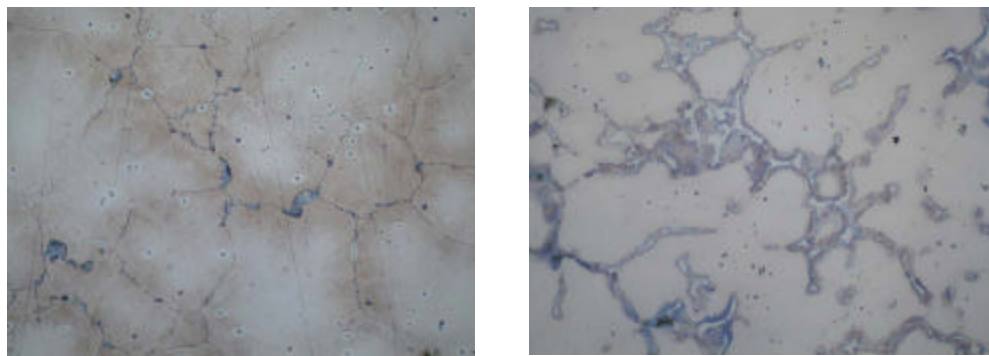


Fig.3 Binary diagram of the Al-Mg system



a)

b)

Fig.4 Microstructure of a) AZ91 Mg alloy and of b) AZ63HP Mg alloy

Etching: 0.5 % Nital, mag. 100 X

The microstructures of the Mg-alloys are shown in Figs. 2 and 3. Polyedric grains of the δ -phase, that is the solid solution Al in Mg, are formed in both alloys. The $\gamma+\delta$ eutectic is segregated in various forms at grain boundaries: i) in a chain form in AZ91 and ii) in a continual

form in AZ63HP. The areas of secondary segregated γ -phase are also visible in the AZ63HP alloy.

3. FATIGUE CRACK GROWTH CHARACTERIZATION

The resistance to fatigue damage development of structural materials is best characterized using the fracture mechanics approach. Fatigue crack growth (FCG) experiments using small cracked specimens of the two Mg-alloys examined in this work were performed and the response in the Paris's regime and at the near-threshold level determined. The special loading apparatus to be mounted in the testing machine is shown in Fig. 5a. Small $25 \times 25 \times 3 \text{ mm}^3$ single-edge-notched coupons were tested, Fig. 5b. The back-face-strain-gage technique was used to monitor continuously the crack length during the tests, [6]. Load vs. back face strain plots, Fig. 5c, were recorded during the test in order to highlight evidence of anticipated crack closure.[7]

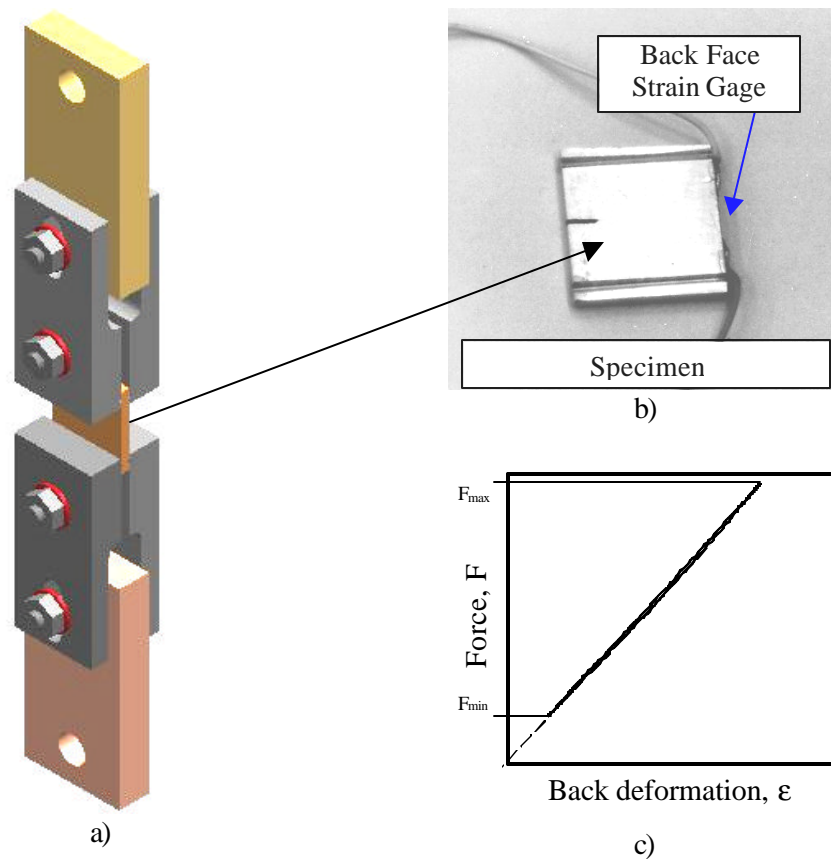


Fig. 5 – Fatigue crack growth testing

a) loading rig, b) specimen, c) typical force-back face strain plot showing compliance of the cracked specimen

Constant amplitude FCG test results for the AZ91 are shown in Fig. 6. Two R-ratios are considered to assess the role of closure mechanisms. It is observed that the difference in the data is limited although a trend showing an inverted response at high and low ΔK is noticeable.

Analogous test results for the AZ63 Mg-alloy are shown in Fig. 7. Similar trends are found although the scatter is higher than in the previous alloy. Details of microstructure and crack growth performance are discussed elsewhere, [8]. When the FCG behaviour of the two alloys is compared, the AZ91 alloy shows a slightly superior performance in with respect to the AZ63 alloy. This latter Mg-alloy shows also a lower toughness.

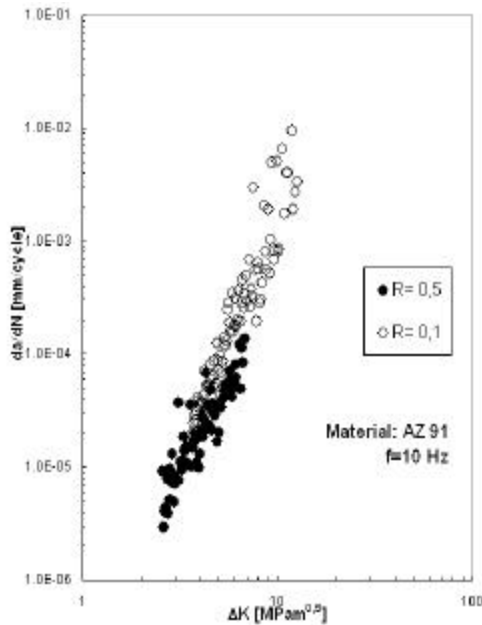


Fig. 6 – Fatigue crack growth testing for the Mg-alloy AZ91

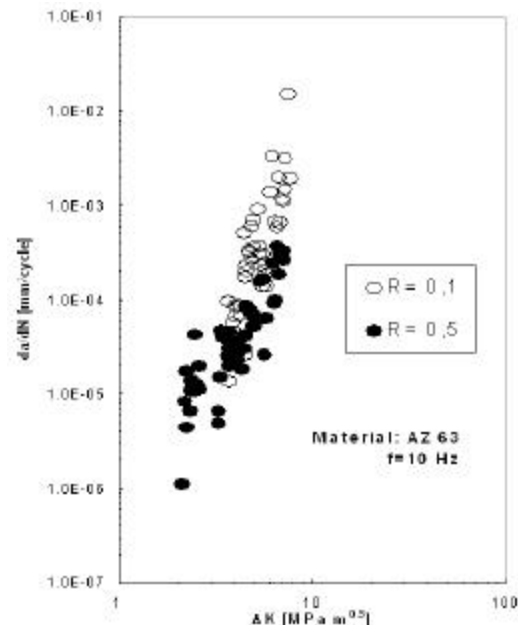


Fig. 7 – Fatigue crack growth data for Mg-alloy AZ63

The data of Figs. 6 and 7 also show that at low crack growth rates R=0.5 data are to the left of the R=0.1 data. This is an indication that under this condition some closure mechanism may be activated. In [8] it was shown that roughness-induced closure may be activated by the relatively large grain sizes of these materials because crack tip deflection is favoured, [9]. The difference in response of the two alloys, however, is limited near the threshold level as shown by the ΔK_{th} data for two R-ratios given in Tab.2. Interestingly, the ΔK_{th} data in Mg-alloys is in line with what is found in Al-alloys under analogous testing conditions.

Tab. 2-Load ratio effect on threshold response of two Mg-alloys

Mg-Alloys	ΔK_{th} (MPa \sqrt{m})	
	R=0.1	R=0.5
AZ63	2.8	1.8
AZ91	2.7	2.0

4. CORROSION RESISTANCE TESTS

Two types of corrosion tests were carried out in four different water environments. The sample immersion test and the potentiodynamic test were used together with i) normal water, ii) distilled water, iii) river water and iv) simulated seawater (3% water solution NaCl).

4.1 Immersion tests

Corrosion resistance of materials is measured by *immersing tests* in different environments. This is most simple way to determining corrosion behaviour. The conditions, which are defined in [10] must be kept during immersion tests. Prismatic samples ($40 \times 20 \times 2 \text{ mm}^3$) were cleaned, degreased and weighted on an analytical balance (measuring accuracy $\pm 0,0001 \text{ g}$) before the tests. Tests in river, normal and distilled water lasted 42 days. Tests in 3% NaCl water solution were interrupted after 7 days because of sample dissolution. The corrosion products on sample surfaces were removed by standard procedures [10,11] after the tests and samples weighted. Corrosion rates in the various environments were determined as the rate of weight loss per unit surface area and are presented in Tab. 2

Tab.2 -Corrosion rates of Mg-alloys after 42 days of immersion tests

Mg-alloy	Corrosion rates [$\text{g.cm}^2.\text{s}^{-1}$]		
	River water	Normal water	Distilled water
AZ91	$1,217.10^{-9}$	$1,179.10^{-9}$	$7,785.10^{-10}$
AZ63HP	$9,324.10^{-9}$	$1,180.10^{-9}$	$2,643.10^{-9}$

From these tests it was determined that corrosion rate of AZ63HP alloy is markedly higher than that of AZ91 alloy. This was caused by the creation of corrosion microcells between microstructural parts (δ phase and γ phase). Corrosion products on the magnesium base formed on the surface of AZ91 alloy (MgO , $\text{Mg}(\text{OH})_2$). These products are not stable in water solutions and surfaces are attacked at oxides or hydroxides discontinuities. On the surface of AZ63HP alloy corrosion products on the magnesium-aluminium base formed $(\text{MgAl})_x \text{O}_y$, $(\text{Al, Mg})_m (\text{OH})_n$ thus interrupting the protective surface film (MgO or $\text{Mg}(\text{OH})_2$). Surface attack by water or water solution is thus favoured, [12].

The mechanisms of corrosion are the same in normal and river water only the surface products differ. The chemical composition of the corrosion products depends on chemical composition of the water and they can accelerate or reduce corrosion. When compared with distilled water results, corrosion rates in normal water are increasing in AZ91 and decreasing in AZ63HP while in river water they increase in both alloys.

4.2 Potentiodynamic tests

Potentiodynamic tests were carried out on Model 350A corrosion measuring system. The characterization of metal sample required the determination of the basic current – potential relationship. The following testing conditions were used: initiation time 30 s (time between sample immersion into the corrosion environment and measurement initiation), temperature $23 \pm 2^\circ\text{C}$, measurement velocity 0.3 mV.s^{-1} , measurement area 1 cm^2 , reference electrode - saturated calomel electrode (SCE).

The corrosion curves of potentiodynamic tests in the four environments (distilled, normal, river and simulated sea water) are shown in Fig. 4 Corrosion characteristics (corrosion potentials E_{corr} and corrosion current I_{corr}) are determined from these curves and are summarized in Tab. 3. Rates of uniform corrosion (v_{corr}) from corrosion currents were calculated according to the Faraday's law

$$v_{\text{corr}} = \frac{I_{\text{corr}} \cdot M}{n \cdot F}$$

where M is the grammolecular weight ($24,4\text{g}\cdot\text{mol}^{-1}$), n is the number of replaced electrons (2) and F is the Faraday's constant ($9,6\cdot 10^4\text{ C}$) and are reported in Tab. 4.

Tab.3- Potentiodynamic characteristics I_{corr} and E_{corr} of corrosion tests

Environment	AZ91		AZ63HP	
	I_{corr} [A.cm ²]	E_{corr} [V]	I_{corr} [A.cm ²]	E_{corr} [V]
Distilled water	$5,0600\cdot 10^{-7}$	-1,3243	$2,5933\cdot 10^{-7}$	-1,3305
Normal water	$1,1509\cdot 10^{-5}$	-1,4847	$2,2800\cdot 10^{-5}$	-1,4620
River water	$1,3877\cdot 10^{-5}$	-1,4473	$1,8910\cdot 10^{-5}$	-1,4540
Simulated sea water	$2,0097\cdot 10^{-4}$	-1,5245	$9,5330\cdot 10^{-5}$	-1,5390

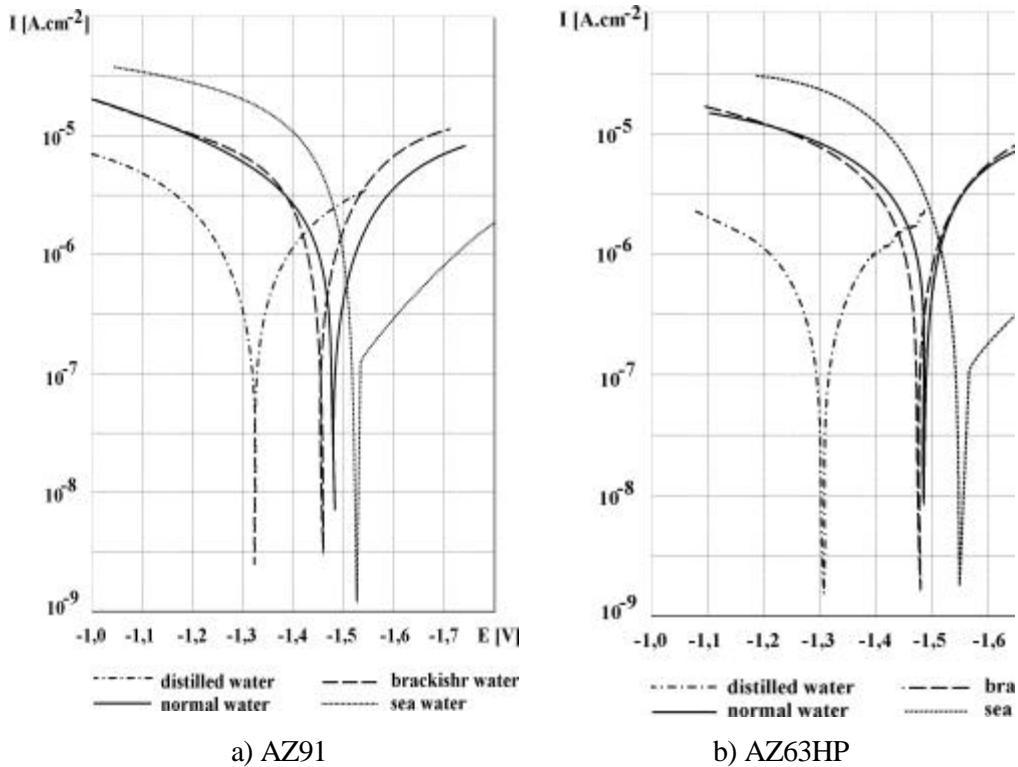


Fig.4 Potentiodynamic curves of Mg-alloys in different environments

Tab.4 - Corrosion rates v_{corr} on corrosion potential E_{corr}

Environment	Corrosion rates v_{corr} [g.cm ² .s ⁻¹]	
	AZ91	AZ63HP
Distilled water	$6,43\cdot 10^{-11}$	$3,30\cdot 10^{-11}$
Normal water	$1,46\cdot 10^{-9}$	$2,90\cdot 10^{-9}$
River water	$1,76\cdot 10^{-9}$	$2,40\cdot 10^{-9}$
Simulated sea water	$2,55\cdot 10^{-8}$	$1,21\cdot 10^{-8}$

The most positive corrosion potentials were measured in distilled water. They were found to decrease in river and normal water and reached the most negative potential values in simulated seawater. The highest corrosion currents, paralleling the highest corrosion rates, were measured in simulated seawater. The corrosion currents in river and normal water were one place value lower as in simulated seawater and lowest corrosion currents were found in distilled water. Aggressive chlorides produced corrosion holes in simulated seawater and the corrosion holes exposed new active surfaces.

The potentiodynamic tests show only the behaviour of Mg-alloys at the beginning of the immersion tests but they cannot identify the structural changes on the specimen surfaces. The corrosion products, which form during immersion tests on the specimen surface, may increase or decrease corrosion rates. The most significant differences were found on AZ63HP alloys tested in distilled water. The active surfaces increased during immersion tests because surface structural components were removed, [12].

5. CONCLUSIONS

Fatigue crack growth test and corrosion tests on two Mg-alloys were conducted and their results reported here. The main conclusions of the fatigue crack growth tests are:

- Both AZ63HP and AZ91 Mg-alloys show a limited influence of the R-ratio on the fatigue crack growth response in the Paris's law regime, although the AZ63HP reveals a larger scatter in the data.
- Closure phenomena appear to play a limited role, although crack advance through the microstructure is fairly irregular especially at low ΔK .
- Threshold values of the ΔK are also similar for the two Mg-alloys with limited influence of the R-ratio. These values are comparable to those measured in Al-alloys.

The main conclusions of the corrosion tests are:

- Corrosion rates of AZ63HP alloy are markedly higher than corrosion rates of AZ91 alloy and an explanation based on the surface corrosion products behavior was presented.
- Corrosion rates in AZ91 alloy and in AZ63HP alloy increase going from the distilled water, to the normal water and to the river water.
- Corrosion potentials and corrosion currents obtained in potentiodynamic tests coherently showed inverse behavior in the four environments: distilled water, normal water, river water and simulated sea water.

ACKNOWLEDGEMENTS

B.H. and P.P. acknowledge the support to this study by the Scientific Grant Agency of Ministry of Education of Slovak Republic and Slovak Academy of Sciences, grant No. 1/8056/01. G.N. acknowledges partial support of this research by CETRA program at University of Zilina, Slovakia.

REFERENCES

- [1] B.L. Mordike, T. Ebert, "Magnesium Properties- applications- potential", *Materials Science and Engineering*, A302, 2001, pp.37 - 45
- [2] Y. Kobayashi, T. Shibusawa, K. Ishikawa, "Environmental effect of fatigue crack propagation of magnesium alloy", *Materials Science and Engineering*, A234 – 236, 1997, 220 - 222
- [3] B. Hadzima, P. Palcek, "Korózna odolnost zliatin horcika" (Corrosion resistance of Madnesium alloys), *Materiálové inžinierstvo*, 3/2001, Žilina.
- [4] J.L. Murray, "Aluminium – Magnesium", ASM International's Binary Alloy Phase Diagrams, Second Edition, Vol.1, USA.
- [5] D.A. Petrov, "Aluminium-Magnesium-Zinc", Ternary Alloys: A Comprehensive Compendium of Evaluated Constitutional Data and Phase Diagrams, Vol.8, 1993
- [6] G. Nicoletto, A. Pirondi, "Experience with fatigue crack growth monitoring techniques", *Materialove inžinierstvo*, Vol.4, No. 9, University of Zilina, Slovakia, 1997, pp.10-16
- [7] A. Saxena, "Computer controlled decreasing stress intensity technique for fatigue crack growth testing" *Journal of Testing and Evaluation*, 6, 1978, pp. 167-174
- [8] P. Lanfredi Sofia, Propagazione di fessure di fatica nelle leghe di magnesio, Thesis in Mechanical Engineering, University of Parma, 2001
- [9] J. Gray, J. Williams, W. Thomson, "Roughness- induced crack closure: an explanation for microstructurally sensitive fatigue crack growth", *Metallurgical Transaction A14*, 1983, pp. 421 – 433
- [10] B. Hadzima, Korózna odolnost zliatin horcika (Corrosion resistance of Magnesium alloys). project of PhD Dissertation, SĽF ŽU v Žiline, 2001
- [11] G.L. Song, A. Atrens, "Corrosion Mechanisms of Magnesium alloys", *Advanced Engineering Materials*, 1, No.1, 1999
- [12] B. Hadzima, P. Palcek, V. Gärtnerová, "The metallographical evaluation of corrosion properties of Mg-Al-Zn alloys", *Acta Metallurgica Slovaca*, special issue 1/2001, 7, 2001, pp. 481-483